AJNR

Comparing Perfusion Metrics Obtained from a Single Compartment Versus Pharmacokinetic Modeling Methods Using Dynamic Susceptibility Contrast-Enhanced Perfusion MR Imaging with Glioma Grade

M. Law, R. Young, J. Babb, M. Rad, T. Sasaki, D. Zagzag and G. Johnson

Comparing Perfusion Metrics Obtained from a Single Compartment Versus Pharmacokinetic Modeling Methods Using Dynamic Susceptibility Contrast-Enhanced Perfusion MR Imaging with Glioma Grade

ORIGINAL RESEARCH

M. Law
R. Young
J. Babb
M. Rad
T. Sasaki
D. Zagzag
G. Johnson

BACKGROUND AND PURPOSE: Numerous different parameters measured by perfusion MR imaging can be used for characterizing gliomas. Parameters derived from 3 different analyses were correlated with histopathologically confirmed grade in gliomas to determine which parameters best predict tumor grade.

METHODS: Seventy-four patients with gliomas underwent dynamic susceptibility contrast-enhanced MR imaging (DSC MR imaging). Data were analyzed by 3 different algorithms. Analysis 1 estimated relative cerebral blood volume (rCBV) by using a single compartment model. Analysis 2 estimated fractional plasma volume (V_p) and vascular transfer constant (K^{trans}) by using a 2-compartment pharmacokinetic model. Analysis 3 estimated absolute cerebral blood flow (CBF), cerebral blood volume (CBV), and mean transit time (MTT) by using a single compartment model and an automated arterial input function. The Mann-Whitney U test was used make pairwise comparisons. Binary logistic regression was used to assess whether rCBV, V_p, K^{trans}, CBV, CBF, and MTT can discriminate high- from low-grade tumors.

RESULTS: rCBV was the best discriminator of tumor grade/type, followed by CBF, CBV, and K^{trans}. Spearman rank correlation factors were the following: rCBV = 0.812 ($P <$ .0001), CBF = 0.677 ($P <$ .0001), CBV = 0.604 ($P <$ .0001), K^{trans} = 0.457 ($P <$ .0001), V_p = 0.301 ($P =$.009), and MTT = 0.089 ($P =$ .448). rCBV was the best single predictor, and K^{trans} with rCBV was the best set of predictors of high-grade glioma.

CONCLUSION: rCBV, CBF, CBV K^{trans}, and V_p measurements correlated well with histopathologic grade. rCBV was the best predictor of glioma grade, and the combination of rCBV with K^{trans} was the best set of metrics to predict glioma grade.

BRAIN

ORIGINAL RESEARCH

Tumors of glial origin are among the most common primary brain tumors. They are typically classified into 1 of the World Health Organization (WHO) grades: low grade (grade II), anaplastic grade (grade III), or glioblastoma (grade IV).[1,2] The grading of gliomas has great clinical significance because high-grade gliomas are usually treated with adjuvant radio- or chemotherapy after resection, whereas low-grade gliomas are not. However, the current reference standard for tumor grading, histopathologic assessment, has limitations such as inherent sampling error associated with the limited number of biopsy samples.[3] Even with cytoreductive surgery, histology can only be performed on excised tumor and residual tumor tissue cannot be examined. Furthermore, the histopathologic classification of gliomas itself is a controversial subject, under constant discussion and revision.[2]

Dynamic susceptibility–weighted contrast-enhanced perfusion MR imaging (DSC MR imaging) of the brain provides hemodynamic information on intracranial neoplasms that complements the anatomic information attainable with conventional MR imaging. Perfusion MR imaging methods exploit signal-intensity changes that occur with the passage of paramagnetic contrast (gadopentetate dimeglumine) through the cerebrovascular system and can be used to derive a number of perfusion metrics related to blood volume and blood flow.[4] Vascular morphology and the degree of angiogenesis are important elements for evaluating tumor type and determining the aggressiveness of intracranial neoplasms. MR imaging measurements of relative cerebral blood volume (rCBV) have been shown to correlate with both conventional angiographic assessments of tumor vascularity and histologic measurements of tumor neovascularization. MR imaging measurements of tumor hemodynamics are, therefore, potentially useful in characterizing tumors because tumor aggressiveness and growth are associated with neovascularization.[5]

rCBV measurements have been shown to correlate reliably with tumor grade and histologic findings of increased tumor vascularity.[4,6-17] Arterial spin-labeling techniques have also been used to investigate gliomas.[18,19] Although arterial spin-labeling was adequate for the distinction between high- and low-grade gliomas, it underestimated blood flow at low-flow rates.[19] Shin et al[14] found that the relative cerebral blood flow (CBF) ratio and rCBV ratio are useful for discriminating high- and low-grade gliomas.

In the present study, we compared 3 different approaches to analyzing DSC MR imaging for assessment of glioma grade. Analysis 1 is based on the intravascular indicator dilution theory and assumes that the contrast agent is confined to the vasculature. Although this assumption is not generally valid, the data can be corrected for contrast leakage. This approach yields rCBV measurements expressed relative to normal contralateral white matter. Analysis 2 is based on a 2-compartment pharmacokinetic model[20,21] and yields not only an estimate of blood plasma volume (V_p) but also the vascular transfer constant (K^{trans}) that describes the permeability of blood vessels to contrast. Analysis 3, also based on the intravascular indicator dilution theory, yields absolute measurements of cerebral blood volume (CBV), CBF, and mean transit time (MTT) but requires estimation of the arterial input function (AIF).

These 3 methods are currently used in clinical practice and are becoming adopted by the major manufacturers in their postprocessing methods. However, to our knowledge, no comparison of the different approaches in identifying tumor grade has been investigated.

Methods

Patients and Histopathologic Analysis

This was a retrospective analysis of patients with a diagnosis of primary intracranial glioma who underwent MR imaging examination at our institution between November 1999 and July 2002. A total of 73 patients had preoperative conventional MR imaging and DSC MR imaging data suitable for evaluation. The ages of the patients ranged from 4 to 85 years with a mean age of 42 years. There were 47 men and 26 women. Approval for this study was obtained from the Institutional Board of Research Associates. The patients did not require informed consent because the studies represented part of their clinical evaluation, and a retrospective waiver of consent was obtained for review of the images and charts from our institutional review board. The entire study was Health Insurance Portability and Accountability Act compliant.

Histopathologic evaluation was performed by an experienced neuropathologist and was based on the WHO classification of gliomas[1]: grade II = low grade glioma ($n = 31$), grade III = anaplastic astrocytoma ($n = 16$), and grade IV = glioblastoma multiforme ($n = 26$). Within the low-grade glioma group ($n = 31$), there were 21 low-grade gliomas and 10 low-grade oligodendrogliomas. Pilocytic astrocytomas were not included in this study because they are classified as a WHO grade I neoplasms and the nodule of enhancement often seen with these tumors demonstrates elevated rCBV and permeability, putting these tumors into a different group of lesions in terms of perfusion characteristics. Furthermore, only 4 patients studied were in the pediatric age group, (4 were in the adolescent/young adult age group). The grade III lesions were all anaplastic astrocytomas. Sixteen patients (21.9%, primarily low-grade gliomas) underwent biopsy alone for histologic grading.

Conventional MR Imaging

Imaging was performed on 1.5T systems (Vision or Symphony, Siemens, Erlangen, Germany). A localizing sagittal T1-weighted image was obtained followed by nonenhanced axial T1-weighted spin-echo (TR/TE, 600/14 ms), axial fluid-attenuated inversion recovery (FLAIR; TR/TE/TI, 9000/110/2500 ms), and T2-weighted images (TR/TE, 3400/119 ms). Postcontrast axial T1-weighted imaging was performed following the acquisition of the DSC MR imaging data.

Dynamic Susceptibility–Weighted, Contrast-Enhanced MR Imaging

DSC MR images were acquired with a gradient-echo echo-planar imaging sequence during the first pass of a standard dose (0.1 mmol/kg) bolus of gadopentetate dimeglumine (Magnevist). Seven to 10 sections were selected through the tumor on the basis of T2-weighted and FLAIR images. Imaging parameters were the following: TR/TE, 1000/54 ms; field of view, 230 × 230 mm; section thickness, 5 mm; matrix, 128 × 128; in-plane voxel size, 1.8 × 1.8 mm; intersection gap, 0%–30%; flip angle, 30°; signal intensity bandwidth, 1470 Hz/pixel. Contrast was injected at a rate of 5 mL/s followed by a 20-mL bolus of saline at 5 mL/s. The injection rate was 5 mL/s in all patients, except for the 4 patients in the 0–9 year age group, in whom the injection rate was reduced to 3 mL/s. A total of 60 images was acquired at 1-second intervals with the injection occurring at the fifth image.

Data were transferred to a Linux workstation for off-line perfusion analysis by using programs developed in-house with the IDL programming languages. In all cases contrast agent concentration, C, is first found by using the simple relationship,[22,23]

$$C \propto -\ln\left(\frac{S}{S_0}\right)$$

where S is the signal intensity and S_0 is the prebolus signal intensity. This equation assumes that T1 shortening effects are negligible. This assumption is true in practice because we use a relatively low flip angle to minimize saturation.

The 3 analyses were performed by a board-certified neuroradiologist experienced with perfusion data acquisition at our institution.

Analysis 1: rCBV

Standard algorithms were used to calculate rCBV.[22,23] Briefly, blood volume was estimated by calculating the area under the contrast agent concentration versus time curve and expressed relative to values measured in a region of interest (ROI) in contralateral normal white matter. Color overlay maps of rCBV were calculated. Using the rCBV maps as a guide, we selected 4 ROIs with high rCBV values. The ROI with the highest rCBV was recorded. Relative CBV was calculated within each of these ROIs to improve signal intensity to noise, and the maximum of the 4 measurements was recorded. This method for the measurement of abnormality provides the highest intra- and interobserver reproducibility in rCBV measurements.[24] To minimize confounding factors in rCBV analysis, we kept the size of the ROIs constant (radius = 3.6 mm).

The effects of contrast leakage were reduced by fitting a gamma-variate function, which approximates the curve that would be obtained without recirculation or leakage, to the measured signal intensity versus time curve.[22,23]

Analysis 2: V_p and K^{trans}

First-pass pharmacokinetic modeling[25] was used to analyze the same DSC MR imaging data used to calculate rCBV. First-pass pharmacokinetic modeling uses an exact expression for tissue contrast concentration, assuming that contrast exists in 2 interchanging compartments (plasma and extravascular extracellular space) and yields estimates of blood plasma volume V_p and K^{trans}, a measure of vascular permeability.

Table 1: Measurements for tumors of each type

Glioma Grade/Type	rCBV	VP	K^{trans}	CBF	CBV	MTT
Low-grade glioma	1.61 ± 0.8	0.99 ± 0.7	0.050 ± 0.09	67.37 ± 84.2	2.95 ± 2.4	3.02 ± 1.12
Low-grade ODG	2.03 ± 0.9	1.12 ± 0.5	0.034 ± 0.06	124.05 ± 104.0	4.43 ± 3.4	3.21 ± 1.31
Low: Glioma + ODG	1.75 ± 0.9	1.03 ± 0.7	0.044 ± 0.08	85.66 ± 93.3	3.43 ± 2.8	3.08 ± 1.16
Anaplastic astrocytoma	3.69 ± 1.5	1.30 ± 0.7	0.167 ± 0.20	99.75 ± 37.3	4.92 ± 2.5	2.98 ± 0.82
Glioblastoma multiforme	6.06 ± 2.2	1.86 ± 1.4	0.234 ± 0.23	274.49 ± 430.9	21.68 ± 62.7	3.37 ± 1.45

Note:—Values are expressed as means ± SD. rCBV indicates maximum relative cerebral blood volume; VP, blood plasma volume; K^{trans}, vascular permeability; CBF, absolute cerebral blood flow; CBV, absolute cerebral blood volume; MTT, mean transit time; ODG, oligodendroglioma.

Table 2: *P* values from an exact Mann-Whitney test for all pairwise comparisons among the tumor grades

Tumor Grades Compared	rCBV	VP	K^{trans}	CBF	CBV	MTT
LG glioma : LG ODG	.17	.254	.381	**.017**	.081	.909
LG glioma : ana Astro	**.0002**	.115	**.014**	**.0044**	**.0037**	.86
LG glioma : GBM	**.0001**	**.017**	**.0015**	**.0001**	**.0001**	.439
LG ODG : ana Astro	**.0033**	.637	**.019**	.941	.388	.98
LG ODG : GBM	**.0001**	.204	**.0036**	**.027**	**.0013**	.777
Ana Astro : GBM	**.0009**	.438	.291	**.0027**	**.0009**	.563

Note:—LG indicates low grade; ODG, oligodendroglioma; ana astro, anaplastic astrocytoma; GBM, glioblastoma multiforme; rCBV, maximum relative cerebral blood volume; VP, blood plasma volume; K^{trans}, vascular permeability; CBF, absolute cerebral blood flow; CBV, absolute cerebral blood volume; MTT, mean transit time. Significant *P* values are in bold face type.

Full details of first-pass pharmacokinetic modeling can be found in Johnson et al,[25] and the method will only be summarized here. It can be shown that the total contrast concentration, C_t, is[25]

$$C_t = V_p C_p + K^{trans} \int_0^t C_p(t') \exp\left(- \frac{K^{trans}}{V_e}(t - t')\right) dt'$$

$$V_e \frac{dC_e}{dt} = K^{trans}(C_F - C_e)$$

where V_p and V_e are the fractional plasma and extravascular extracellular space volumes, C_t and C_p are the tracer concentrations in the extravascular extracellular space and plasma respectively, and K^{trans} is the transfer constant.

An estimate of C_p is acquired from a region of normal white matter[26] and fitted to the model function of C_t with K^{trans}, V_e, and V_p as free parameters.

Although it is, in principle, possible to form maps of K^{trans} on a pixel-by-pixel basis, the calculation can be sensitive to noise and is time-consuming. Instead, maps of the fractional signal intensity drop at 25 seconds after the bolus (SD25 maps) were calculated as a surrogate. If vascular permeability is high, residual contrast concentration is also high after the bolus has passed and the SD25 value is also high. The SD25 maps, therefore, provide a simple index related to vascular permeability that can be used to select ROIs for K^{trans} calculation. K^{trans} was calculated in 4 ROIs demonstrating the highest SD25 values, and the maximal value was recorded. V_p from the same region of interest was also recorded.

Analysis 3: Absolute CBV, CBF, and MTT
Absolute CBV, CBF, and MTT were calculated by using the method of Rempp et al.[27,28] These parameters can be calculated from the following equations:

$$MTT = \frac{\int C dt}{C_{max}}$$

$$CBV = \frac{\int C dt}{\int AIP\ dt}$$

$$CBF = \frac{CBV}{MTT}$$

where C is the tissue concentration following an ideal instantaneous bolus and C_{max} is the maximal value of C. The bolus is not instantaneous, of course, but an approximation to the idealized response can be found by deconvolving the measured tissue concentration with the AIF. The AIF was found by using an automated method similar to that described by Rempp et al[27] and Carroll et al.[29] The minimum signal intensity, corresponding to the bolus peak, is found in each pixel within the head. The average signal intensity drop and average bolus arrival time are then calculated for all pixels. Pixels in which the bolus arrives early and in which the signal intensity drop is larger than average are assumed to be within arteries. The AIF was found by averaging the signals from all such pixels.

Statistical Analysis
The mean and standard deviation of each measure for tumors of each type were obtained. For each measure (rCBV, V_p, K^{trans}, CBF, CBV, and MTT), the Mann-Whitney *U* test was applied to the ranks to make all pairwise comparisons among the tumor grades (separating low-grade gliomas from low-grade oligodendrogliomas, given there has been recent evidence to suggest that oligodendrogliomas may have elevated perfusion).[11,30] The associations between each measure were assessed through Spearman rank correlation coefficients. Binary logistic regression was used to assess the diagnostic utility (sensitivity, specificity, and predictive values) of using rCBV, V_p, K^{trans}, CBF, CBV, and MTT to discriminate high- from low-grade gliomas.

Results
The mean and standard deviation of each measure for tumors of each type are presented in Table 1. The results from an exact Mann-Whitney *U* test used to make all pairwise comparisons among the tumor grades are summarized in Table 2. For each measure, the Mann-Whitney *U* test demonstrated rCBV to be the best discriminator of tumor grade and type, followed by CBF, CBV, and K^{trans}. The tumor grades are ordered as low-grade gliomas < anaplastic astrocytoma < glioblastoma multiforme; thus, Table 3 shows the Spearman rank correlation of rCBV, V_p, K^{trans}, CBF, CBV, and MTT with tumor grade. Tumor grade was signif-

Table 3: Spearman rank correlation coefficients with _P_ values

	rCBV	VP	K^{trans}	CBF	CBV	MTT
Correlation	0.81237	0.30173	0.45763	0.67768	0.60417	0.08954
_P_ value	<.0001	.009	<.0001	<.0001	<.0001	.448

Note:—rCBV denotes maximum relative cerebral blood volume; VP, blood plasma volume; K^{trans}, vascular permeability; CBF, absolute cerebral blood flow; CBV, absolute cerebral blood volume; MTT, mean transit time.

Table 4: Selected combinations of sensitivity and specificity achieved (corresponding to points on the receiver operating characteristic curve) on the basis of diagnostic models using K^{trans} and rCBV when considered alone and in combination

rCBV and K^{trans}		rCBV		K^{trans}	
Sensitivity (%)	Specificity (%)	Sensitivity (%)	Specificity (%)	Sensitivity (%)	Specificity (%)
100.0	33.3	100.0	46.7	100.0	0.0
97.7	60.0	97.7	66.7	72.1	40.0
95.3	66.7	95.3	70.0	62.8	66.7
90.7	76.7	88.4	76.7	60.5	70.0
81.4	83.3	86.0	83.3	32.6	86.7
72.1	93.3	83.7	93.3	30.2	90.0
62.8	96.7	74.4	96.7	25.6	93.3
16.3	100.0	69.8	100.0	2.3	100.0

Note:—rCBV indicates maximum relative cerebral blood volume; K^{trans}, vascular permeability.
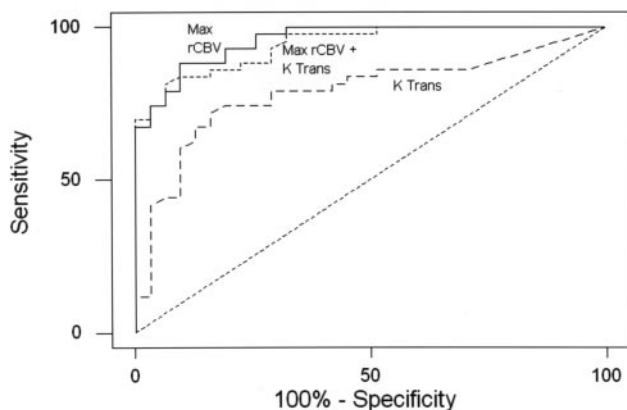

Fig 1. The ROC curves associated with the model to diagnose high-grade tumors on the basis of rCBV, rCBV with K^{trans}, and K^{trans} alone. Diagnostic models based on K^{trans} with rCBV and rCBV alone each had significantly higher ($P < .01$) area under the ROC curve (AUC = 0.94, 0.90, respectively) than did the model based on K^{trans} alone (AUC = 0.63). Max indicates maximum.

Fig 2. Scatterplot of rCBV versus K^{trans} shows true low-grade gliomas as crosses and true high grade gliomas as black points. The figure demonstrates that rCBV and K^{trans} together are good predictors of glioma grade. The performance of the diagnostic model to predict high-grade tumors using both K^{trans} and Max rCBV when overall diagnostic accuracy is highest (sensitivity = 90.7%, specificity = 76.7%) is shown.

icantly positively correlated with each of rCBV, V_p, K^{trans}, CBF, and CBV, but not with MTT. Thus, higher grade tumors tended to be associated with higher values of rCBV, V_p, K^{trans}, CBF, and CBV.

Binary logistic regression and receiver operating characteristic (ROC) curve analyses were used to assess the diagnostic utility of using the metrics to discriminate high-grade (anaplastic astrocytoma and glioblastoma multiforme) from low-grade (low-grade gliomas and low-grade oligodendroglioma) tumors. Table 4 summarizes the stepwise variable selection, declares rCBV to be the best single predictor of high-grade tumors, and identifies K^{trans} and rCBV as the best set of significant independent predictors of tumor grade. Table 4 shows selected combinations of sensitivity and specificity achieved (corresponding to points on the ROC curve) on the basis of diagnostic models based on K^{trans} and rCBV when considered alone and in combination. The ROC area under the curve (AUC) analysis (Fig 1) indicated that the diagnostic models based on K^{trans} with rCBV and rCBV alone each had significantly
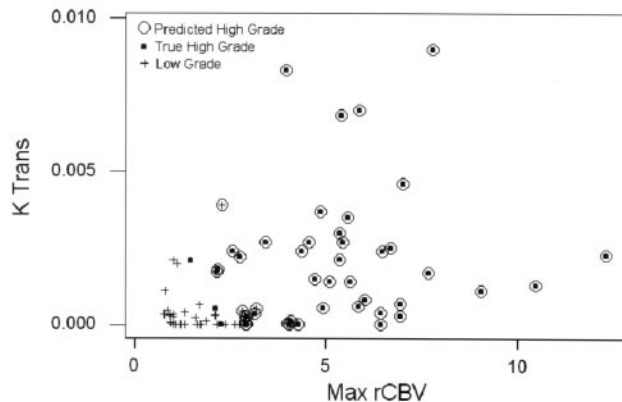
higher ($P < .01$) area under the ROC curve (AUC = 0.94, 0.90, respectively) than did the model based on K^{trans} alone (AUC = 0.63) but were not distinguishable from each other in terms of AUC ($P = .07$). The area under the ROC curve of 0.94 indicates high sensitivity and specificity. The performance of the diagnostic model for the detection of high-grade tumors has a sensitivity of 90.7% and a specificity of 76.7%. This is demonstrated by using a scatterplot of K^{trans} versus rCBV shown in Fig 2. Examples of low-grade glioma, anaplastic astrocytoma, and glioblastoma multiforme with the respective rCBV, SD25, CBF, CBV, and MTT color overlay maps are shown in Figs 3–5.

Discussion

Neovascularization is an important factor in determining glioma grade; the other factors are nuclear atypia, mitoses, and necrosis.[2] DSC MR imaging has shown promise in grading gliomas. In this study, we examined 4 different tumor types: low-grade glioma, low-grade oligodendroglioma, anaplastic astrocytoma, and glioblastoma multi-
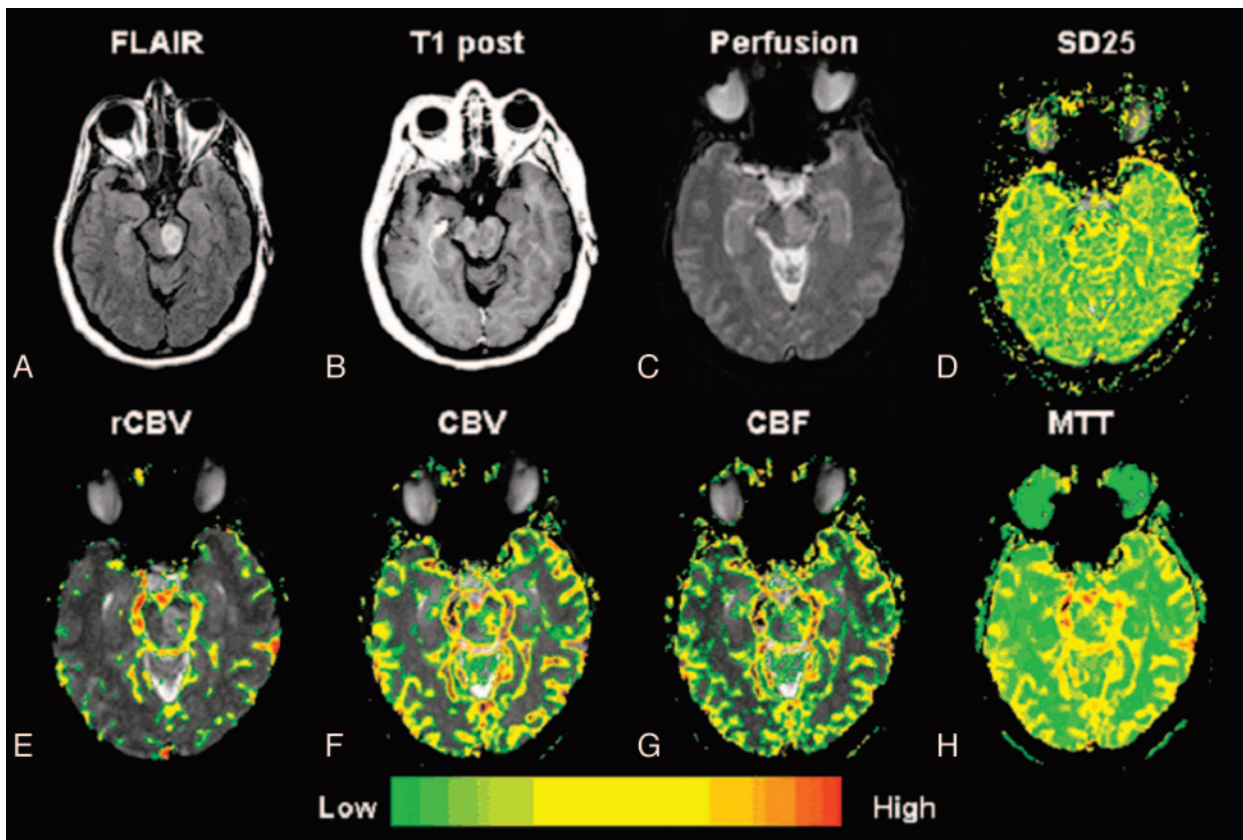
Fig 3. *A–H,* Low-grade astrocytoma (grade II/IV). Top row, left to right.

A, Axial FLAIR image (TR/TE/TI, 9000/110/2500 ms) demonstrates a lesion in the left midbrain with high signal intensity and minor mass effect.

B, Axial T1-weighted postcontrast image (TR/TE, 600/14 ms; 1 excitation) demonstrates no evidence of contrast enhancement, in keeping with a low-grade astrocytoma.

C and *D,* Gradient-echo (TR/TE, 1000/54 ms) axial DSC MR imaging and SD25 color map suggests low permeability throughout the lesion.

E–G, Bottom row (left to right). rCBV, CBV, and CBF maps demonstrate a few foci of mildly elevated rCBV, CBV, and CBF within the glioma.

H, MTT map demonstrates some prolongation in MTT within the tumor.

forme. To distinguish tumor types and grades, rCBV was the best parameter, followed by CBF, CBV, and K^{trans}. rCBV was able to distinguish between all pairs of tumor types except low-grade oligodendroglioma versus low-grade astrocytoma. Absolute CBF could differentiate between all tumor types except low-grade oligodendroglioma versus low-grade astrocytoma. Absolute CBV could differentiate all tumor types except low-grade oligodendroglioma versus anaplastic astrocytoma and low-grade oligodendroglioma versus low-grade astrocytoma. Last, K^{trans} could differentiate all tumor types except low-grade astrocytoma versus low-grade oligodendroglioma and anaplastic astrocytoma versus glioblastoma multiforme. MTT, however, was not successful in distinguishing glioma grades (Table 2). Finding higher rCBV in low-grade oligodendroglioma compared with low-grade astrocytomas (Table 1) is in keeping with recently published data showing elevated rCBV in oligodendrogliomas[11,30] in a study using spin-echo perfusion imaging. The histologic finding in oligodendrogliomas is an attenuated network of branching capillaries that produce a vascular pattern resembling chicken wire in addition to a "fried-egg" appearance and correspond to classic oligodendroglioma histology.[31,32] When correlating individual parameters with glioma grade, we found that rCBV had the highest Spearman correlation factor followed by CBF,

CBV, K^{trans}, and V_p (Table 3). Previous studies have also indicated that rCBV has a high level of correlation with glioma grade at a statistically significant level.[10]

Gliomas, particularly high-grade gliomas, are characterized by bizarre and extreme tortuosity in the morphology of the angioarchitecture. The blood flow and volume can, therefore, be extremely variable and heterogeneous within any given region of a tumor.[33,34] Furthermore, there are multiple factors that influence the leakiness of a blood vessel, including luminal surface area, permeability of the vessel wall, rate of blood flow, and hydrostatic, interstitial, and osmotic gradients across the endothelium,[35-37] not to mention body temperature. Hence, K^{trans}, which includes all these factors, is not simply a measure of vascular permeability. Furthermore, our method of estimating K^{trans} involves a measurement period of only 60 seconds during the first pass of contrast. Consequently, the method is relatively insensitive to slow leakage. In Fig 5, the areas of high SD25 (ie, areas of high leakage during the first pass) do not correspond to enhancing regions on postcontrast T1 images. This finding may reflect a difference between areas of extremely high permeability in which contrast extravasation is limited by flow and areas in which it is limited by vascular permeability. Targeted biopsy samples coregistered with the perfusion maps may help determine which regions cor-
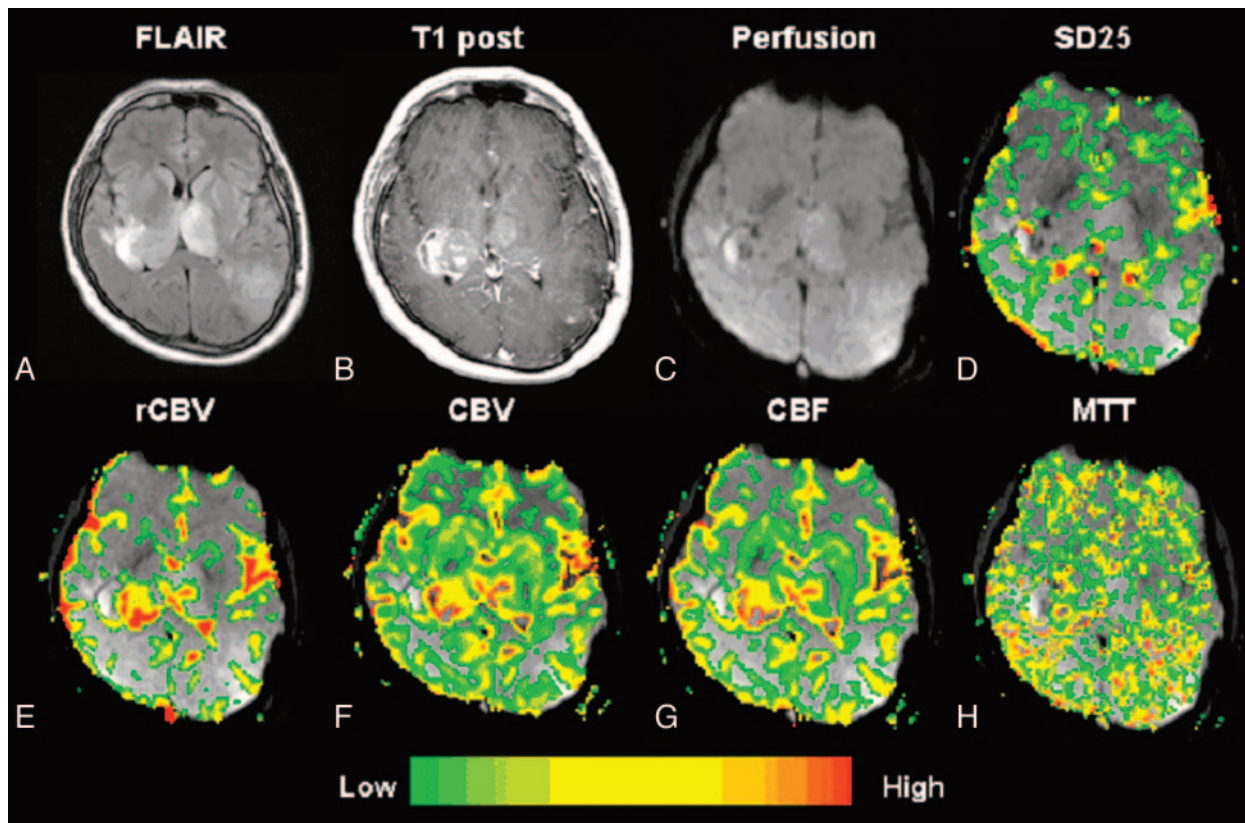
Fig 4. *A–H*, Anaplastic astrocytoma (grade III/IV). Top row, left to right.

A, Axial FLAIR image (TR/TE/TI, 9000/110/2500 ms) demonstrates a dominant lesion in the right thalamus with extension to the left thalamus and parietooccipital region.

B, Axial T1-weighted postcontrast image (TR/TE, 600/14 ms; 1 excitation) demonstrates heterogeneous contrast enhancement in keeping with an anaplastic astrocytoma.

C, Gradient-echo axial DSC MR image (TR/TE, 1000/54 ms).

D, SD25 color map shows foci of increased permeability throughout the lesion.

E–G, Bottom row (left to right). rCBV, CBV, and CBF maps demonstrate elevated rCBV, CBV, and CBF within the glioma.

H, MTT map demonstrates some prolongation in MTT within the tumor.

relate best with angiogenesis. This finding also suggests that the information provided by our first-pass technique may be complementary to that provided by alternative methods that measure K^{trans} during the (steady state) washout of contrast from the tumor.[38-40]

Finding poor correlation between MTT and glioma grade may at first seem surprising; however, there are a number of explanations. MTT merely reflects the time it takes for the bolus peak to transit through a vessel or tissue of interest. As a consequence, it may be prolonged from numerous vascular collaterals or an increase in mean vessel attenuation/diameter as a result of angiogenesis. Conversely, MTT may be decreased as a result of higher flow rates or arteriovenous shunt surgery in a very heterogeneous tumor vascular environment. It is also possible that within both low- and high-grade gliomas, regions of increased blood volume are accompanied by increased blood flow, ultimately having no overall effect on the MTT.

Finally, it might appear surprising that the V_p measurements correlate poorly with tumor grade because they are an estimate of rCBV. However, in previous studies V_p and rCBV were compared in identical ROIs. In this study, V_p was measured in ROIs in which K^{trans} was found to be maximum, and rCBV was measured in ROIs in which rCBV was

found to be maximum. This finding strongly suggests that K^{trans} is elevated in areas in which rCBV (and V_p) is normal and vice versa and hence that the 2 parameters provide independent information, a hypothesis that is confirmed by the finding that K^{trans} and rCBV are independent predictors of tumor grade.

Conclusion

In the present study, rCBV, CBF, CBV, and K^{trans} measurements are shown to correlate well with histopathologic grade. MTT for a number of pathophysiologic reasons does not appear to correlate or be able to discriminate between glioma grades. The combination of rCBV with K^{trans} metrics was shown to be the best set of independent predictors of tumor grade but did not improve the prediction of glioma grade above the predictive value for rCBV alone. There are numerous limitations when using various models and an AIF to calculate perfusion parameters, and it is important in the clinical setting to be aware of these limitations, errors, and artifacts. Regardless, once these limitations are recognized, DSC MR imaging can offer valuable additional information not given by conventional MR imaging, which can aid in preoperative patient management and subsequent follow-up.
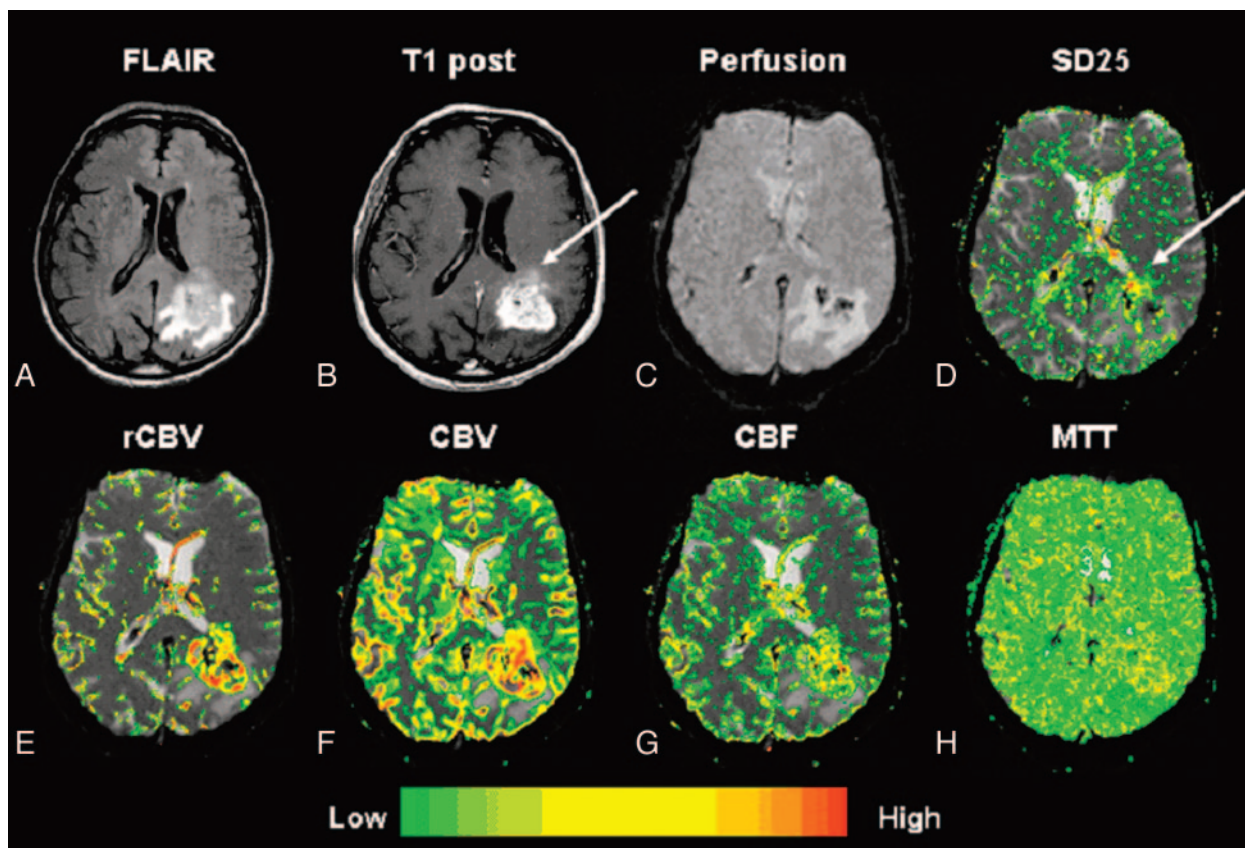
Fig 5. *A–H*, Glioblastoma multiforme (grade IV/IV). Top row, left to right.

A, Axial FLAIR image (TR/TE/TI , 9000/110/2500 ms) demonstrates a lesion with surrounding increased signal intensity in the left parietooccipital region.

B, Axial T1-weighted postcontrast image (TR/TE, 600/14 ms; 1 excitation) demonstrates heterogeneous contrast enhancement in keeping with a glioblastoma multiforme.

C, Gradient-echo axial DSC MR image (TR/TE, 1000/54 ms).

D, SD25 color map shows foci of increased permeability anteriorly in the lesion, which appears to "washout" on the axial postcontrast T1-weighted image (*arrows*), possibly indicating hyperpermeability during the first pass of contrast. The areas of enhancement more posteriorly may reflect more delayed permeability.

E–G, Bottom row (left to right). rCBV, CBV, and CBF maps demonstrate elevated rCBV, CBV, and CBF within the glioblastoma multiforme.

H, MTT map demonstrates some prolongation in MTT within the tumor.

References

1. Kleihues P, Cavanee P. *WHO Classification of Tumors: Pathology and Genetic of Tumours of the Nervous System*. Lyon, France: IARC Press, 2000
2. Daumas-Duport C, Scheithauer B, O'Fallon J, et al. **Grading of astrocytomas: a simple and reproducible method.** *Cancer* 1988;62:2152–65
3. Jackson RJ, Fuller GN, Abi-Said D, et al. **Limitations of stereotactic biopsy in the initial management of gliomas.** *Neuro-oncol* 2001;3:193–200
4. Cha S, Knopp EA, Johnson G, et al. **Intracranial mass lesions: dynamic contrast-enhanced susceptibility-weighted echo-planar perfusion MR imaging.** *Radiology* 2002;223:11–29
5. Burger P. **Malignant astrocytic neoplasms: classification, pathology, anatomy, and response to therapy.** *Semin Oncol* 1986;13:16–20
6. Aronen HJ, Gazit IE, Louis DN, et al. **Cerebral blood volume maps of gliomas: comparison with tumor grade and histologic findings.** *Radiology* 1994;191:41–51
7. Bruening R, Kwong KK, Vevea MJ, et al. **Echo-planar MR determination of relative cerebral blood volume in human brain tumors: T1 versus T2 weighting.** *AJNR Am J Neuroradiol* 1996;17:831–40
8. Knopp EA, Cha S, Johnson G, et al. **Glial neoplasms: dynamic contrast-enhanced T2*-weighted MR imaging.** *Radiology* 1999;211:791–98
9. Law M, Yang S, Babb JS, et al. **Comparison of cerebral blood volume and vascular permeability from dynamic susceptibility contrast-enhanced perfusion MR imaging with glioma grade.** *AJNR Am J Neuroradiol* 2004;25:746–55
10. Law M, Yang S, Wang H, et al. **Glioma grading: sensitivity, specificity, and predictive values of perfusion MR imaging and proton MR spectroscopic imaging compared with conventional MR imaging.** *AJNR Am J Neuroradiol* 2003;24:1989–98
11. Lev MH, Ozsunar Y, Henson JW, et al. **Glial tumor grading and outcome prediction using dynamic spin-echo MR susceptibility mapping compared with conventional contrast-enhanced MR: confounding effect of elevated rCBV of oligodendrogliomas [corrected].** *AJNR Am J Neuroradiol* 2004;25:214–21
12. Lev MH, Rosen BR. **Clinical applications of intracranial perfusion MR imaging.** *Neuroimaging Clin N Am* 1999;9:309–31
13. Petrella JR, Provenzale JM. **MR perfusion imaging of the brain: techniques and applications.** *AJR Am J Roentgenol* 2000;175:207–19
14. Shin JH, Lee HK, Kwun BD, et al. **Using relative cerebral blood flow and volume to evaluate the histopathologic grade of cerebral gliomas: preliminary results.** *AJR Am J Roentgenol* 2002;179:783–89
15. Sugahara T, Korogi Y, Kochi M, et al. **Correlation of MR imaging-determined cerebral blood volume maps with histologic and angiographic determination of vascularity of gliomas.** *AJR Am J Roentgenol* 1998;171:1479–86
16. Sugahara T, Korogi Y, Shigematsu Y, et al. **Value of dynamic susceptibility contrast magnetic resonance imaging in the evaluation of intracranial tumors.** *Top Magn Reson Imaging* 1999;10:114–24
17. Wong ET, Jackson EF, Hess KR, et al. **Correlation between dynamic MRI and outcome in patients with malignant gliomas.** *Neurology* 1998;50:777–81
18. Wolf RL, Wang J, Wang S, et al. **Grading of CNS neoplasms using continuous arterial spin-labeled perfusion MR imaging at 3 Tesla.** *J Magn Reson Imaging* 2005;22:475–82
19. Warmuth C, Gunther M, Zimmer C. **Quantification of blood flow in brain tumors: comparison of arterial spin labeling and dynamic susceptibility-weighted contrast-enhanced MR imaging.** *Radiology* 2003;228:523–32
20. Tofts PS, Kermode AG. **Measurement of the blood-brain barrier permeability and leakage space using dynamic MR imaging: fundamental concepts.** *Magn Res Med* 1991;17:357–67
21. Tofts PS, Brix G, Buckley DL, et al. **Estimating kinetic parameters from dynamic contrast-enhanced T(1)-weighted MRI of a diffusable tracer: standardized quantities and symbols.** *J Magn Reson Imaging* 1999;10:223–32
22. Rosen BR, Belliveau JW, Vevea, et al. **Perfusion imaging with NMR contrast agents.** *Magn Res Med* 1990;14:249–65
23. Rosen BR, Belliveau JW, Buchbinder BR, et al. **Contrast agents and cerebral hemodynamics.** *Magn Reson Med* 1991;19:285–92

24. Wetzel SG, Cha S, Johnson G, et al. **Relative cerebral blood volume measurements in intracranial mass lesions: interobserver and intraobserver reproducibility study.** *Radiology* 2002;224:797–803

25. Johnson G, Wetzel S, Cha S, et al. **A new approach to measuring blood volume and vascular transfer constant from dynamic, contrast-enhanced MRI.** *Magn Res Med* 2004;51:961–68

26. Leenders KL, Perani D, Lammertsma AA, et al. **Cerebral blood flow, blood volume and oxygen utilization: normal values and effect of age.** *Brain* 1990; 113(Pt 1):27–47

27. Rempp KA, Brix G, Wenz F, et al. **Quantification of regional cerebral blood flow and volume with dynamic susceptibility contrast-enhanced MR imaging.** *Radiology* 1994;193:637–41

28. Ostergaard L, Weisskoff RM, Chesler DA, et al. **High-resolution measurement of cerebral blood flow using intravascular tracer bolus passages. Part I. Mathematical approach and statistical analysis.** *Magn Reson Med* 1996; 36:715–25

29. Carroll TJ, Rowley HA, Haughton VM. **Automatic calculation of the arterial input function for cerebral perfusion imaging with MR imaging.** *Radiology* 2003;227:593–600

30. Cha S, Tihan T, Crawford F, et al. **Differentiation of low-grade oligodendrogliomas from low-grade astrocytomas by using quantitative blood-volume measurements derived from dynamic susceptibility contrast-enhanced MR imaging.** *AJNR Am J Neuroradiol* 2005;26:266–73

31. Engelhard HH, Stelea A, Cochran EJ. **Oligodendroglioma: pathology and molecular biology.** *Surg Neurol* 2002;58:111–17

32. Watanabe T, Nakamura M, Kros JM, et al. **Phenotype versus genotype correlation in oligodendrogliomas and low-grade diffuse astrocytomas.** *Acta Neuropathol (Berl)* 2002;103:267–75

33. McDonald DM, Choyke PL. **Imaging of angiogenesis: from microscope to clinic.** *Nat Med* 2003;9:713–25

34. Vajkoczy P, Menger MD. **Vascular microenvironment in gliomas.** *J Neurooncol* 2000;50:99–108

35. McDonald DM, Blank P. **Significance of blood vessel leakiness in cancer.** *Cancer Res* 2002;62:5381–85

36. Li KL, Zhu XP, Checkley DR, et al. **Simultaneous mapping of blood volume and endothelial permeability surface area product in gliomas using iterative analysis of first-pass dynamic contrast enhanced MRI data.** *Br J Radiol* 2003;76: 39–51

37. Harrer JU, Parker GJ, Haroon HA, et al. **Comparative study of methods for determining vascular permeability and blood volume in human gliomas.** *J Magn Reson Imaging* 2004;20:748–57

38. Roberts HC, Roberts TP, Bollen AW, et al.. **Correlation of microvascular permeability derived from dynamic contrast-enhanced MR imaging with histologic grade and tumor labeling index: a study in human brain tumors.** *Acad Radiol* 2001;8:384–91

39. Roberts HC, Roberts TP, Ley S, et al. **Quantitative estimation of microvascular permeability in human brain tumors: correlation of dynamic Gd-DTPA-enhanced MR imaging with histopathologic grading.** *Acad Radiol* 2002;9 (suppl 1):S151–155

40. Roberts HC, Roberts TPL, Brasch RC, et al. **Quantitative measurement of microvascular permeability in human brain tumors achieved using dynamic contrast-enhanced MR imaging: correlation with histologic grade.** *AJNR Am J Neuroradiol* 2000;21:891–99